Thin Solid Films 519 (2010) 700–705

Contents lists available at ScienceDirect

Thin Solid Films

journal homepage: www.elsevier.com/locate/tsf

Carbon fiber coating with silver using intervening Au/Pd nanoparticle films produced using a spark discharge

Jeong Hoon Byeon [a], Jang-Woo Kim [b,*]

[a] LCD Division, Samsung Electronics Co., Ltd., Yongin 446-711, Republic of Korea
[b] Department of Digital Display Engineering, Hoseo University, Asan 336-795, Republic of Korea

ARTICLE INFO

Article history:
Received 24 May 2010
Received in revised form 14 August 2010
Accepted 19 August 2010
Available online 26 August 2010

Keywords:
Catalytic surface activation
Electroless silver deposition
Gold aerosol nanoparticles
Flat silver film

ABSTRACT

A low roughness conductive silver film on a fiber substrate was fabricated via a catalytic surface activation (needed to initiate electroless silver deposition) with spark produced gold aerosol nanoparticles. Gold had a similar lattice parameter with silver in crystallinity and thus a crystallographic misfit between gold activated substrate and silver was minimized during the deposition, resulting in formation of a flat silver film. Properties were compared with those obtained with palladium aerosol activation, the gold activation enhanced thin-metallic film properties in surface root-mean-square roughness (nm: 8, gold vs 44, palladium) and electrical resistivity (μΩ cm: 64, gold vs 498, palladium) at 88 mg/g (silver/substrate) in deposition amount.

1. Introduction

Metal deposited carbon fibers are superior to undeposited carbon fibers in providing fiber-matrix composites of high electrical conductivity, since the electrical resistivity of metal is much lower than that of a carbon fiber [1]. Therefore, the composites can be used in various applications, such as electromagnetic interference shielding materials [2], electrolysis cells [3], conductive fillers [4], and etc. Current metal deposition techniques on a fibrous substrate are conductive paints and lacquers, sputter coating, vacuum deposition, flame and arc spraying, and electroless deposition (ELD) [5]. Among them, ELD has advantages, such as coherent metal deposition, excellent conductivity, and applicability to complex-shaped nonconductor materials.

The low electrical resistivity of silver and the relatively simple procedure of its ELD generate an interest in micro-/nanoelectronics, etc. On the other hand, there is at least one serious problem which remains to be resolved. Initiation of the ELD process is preceded by surface activation to provide the catalytic sites on a substrate [6]. The traditional method for ELD most commonly uses wet tin-sensitization and palladium-activation steps for this purpose [7]. During the ELD on a surface activated by palladium, the deposited silver is agglomerated together [8], it is still difficult to control the surface uniformity of the electroless deposited silver film. The traditional palladium activations [9,10] require long process times and wet chemical processes involve the loss of expensive metal ions and create environmental pollution problems [11]. One alternative to fabricate uniform film is attempted using silver–tungsten species [9,12]. However, because tungsten as an impurity is the main source of high resistivity, it is essential that only silver is deposited. Moreover, this approach still use wet chemical activation steps, and thus it is still necessary to activate the substrate surface with simple, effective, and environmentally friendly methods.

As shown in Table 1, there is a lattice misfit of 5% between palladium and silver. This fact can make the aggravated bonding between silver and palladium. Therefore, the substitution of the traditional activation material by gold having more similar lattice parameters than palladium is expected to improve the bonding between silver and activated substrate, which may prevent agglomeration of silver on the substrate [8]. In this regard, recently we fabricated a pure, uniform electroless silver film using ultrafine silver aerosol particle [13]. As an expansion of a previous study, in this paper, spark produced gold aerosol nanoparticles were applied to activate a fibrous carbon substrate for use in ELD to form flat silver film. For comparison purposes, the surface of another substrate was activated by palladium aerosol nanoparticles.

2. Materials and methods

The proposed catalytic surface activation (Fig. 1a) involved the spark discharge [14,15] of gold (or palladium) aerosol nanoparticles and their filtration by porous carbon fiber (PCF) substrate. A spark was formed between two identical gold (or palladium) rods (diameter: 3 mm, length: 100 mm, Nilaco, Japan) inside a reactor (volume: 42.8 cm^3) under a pure nitrogen environment (less than 10^{-4} impurities) at standard temperature and pressure. The spark discharge is a kind of atmospheric nonequilibrium plasmas [16]. While the collision rate of electrons, ions, and neutrals is high, the discharge does

* Corresponding author. Tel.: +82 41 540 5925; fax: +82 41 540 5929.
E-mail address: jwkim@hoseo.edu (J.-W. Kim).

0040-6090/$ – see front matter © 2010 Elsevier B.V. All rights reserved.
doi:10.1016/j.tsf.2010.08.121

Table 1
Crystal structure, lattice parameter, resistivity, and binding energy of elemental metals.

Element	Crystal structure	Lattice parameter (nm)	Resistivity (μΩ cm)	Binding energy (kJ/mol)
Copper	fcc	0.362	1.7	Gold–silver: 202.9
Palladium		0.389	10.7	Palladium–silver: 185.0
Silver		0.409	1.6	Silver–silver: 160.3
Gold		0.408	2.4	

not reach thermal equilibrium because it is short-lived, being interrupted before an arc discharge [17]. The flow rate of nitrogen gas, which was controlled using a mass flow controller (MKS), was set to 3 L/min. The electrical circuit specifications of spark are as follows: a resistance of 0.5 MΩ, a capacitance of 10 nF, a loading current of 2 mA, an applied voltage of 3.0 kV, and a frequency of 667 Hz. For reference, metal nanoparticles can also be produced at rates of several mg/h by an arc discharge under high power, about 1 kW (several tens A at several V) [18].Thus, the arc method occasionally induces a large proportion of unwanted products (e.g. agglomerates) due to the harsh production condition arising from the high energy generated during the process [19]. PCF has less electrical conductivity than CF because of the very large number of micropores on its surface. Therefore, metal deposited PCF substrates can be manufactured with various levels of conductivity, depending on the preparation method.

Once the substrate was activated by a preliminary deposition of gold (or palladium) aerosol nanoparticles, the substrate was immersed in a silver ELD bath for the deposition of silver onto the surface of the activated substrate (Fig. 2a). The silver ELD bath (maintained at 25 °C) was a mixture of solutions A and B at a 1:1 (v/v) ratio. Solution A contained 4 g of $AgNO_3$, 80 g of $C_{10}H_{14}N_2Na_2O_8 \cdot 2H_2O$, 88 mL of isopropyl alcohol, 12 mL of acetic acid, and 400 mL of NH_4OH in 1 L of DI water. Solution B contained 4 mL of hydrazine, 1 mL of mercerine, and 400 mL of ethyl alcohol in 1 L of deionized water.

The size distribution of the gold (palladium) aerosol nanoparticles was measured using a scanning mobility particle sizer (SMPS) consisting of an electrostatic classifier (TSI 3085), ultrafine condensation particle counter (TSI 3025), and aerosol charge neutralizer (NRD 2U500). The SMPS system, which measures the mobility equivalent diameter, was operated at a sample flow of 0.3 L/min, a sheath flow of 3 L/min, and a scan time of 180 s (measurement range: 4.61–157 nm). The morphology and microstructure of the spark produced nanoparticles were analyzed by the high resolution transmission electron microscopy (TEM, JEM-3010) operated at 300 kV. Field-emission scanning electron microscope (SEM, JSM-6500F, JEOL) images and energy dispersive X-ray (EDX, JED-2300, JEOL) profiles were obtained at an accelerating voltage of 15 kV. The amount of deposited silver on the PCF was determined by inductively coupled plasma atomic emission spectroscopy (ICPAES, Elan 6000, Perkin–Elmer). X-ray diffraction (XRD) studies of the silver deposited PCF were carried out on a Rigaku RINT-2100 diffractometer equipped with a thin-film attachment using Cu-$K\alpha$ radiation (40 kV, 40 mA). The 2θ angles ranged from 10 to 90° at 4°/min by step scanning at an

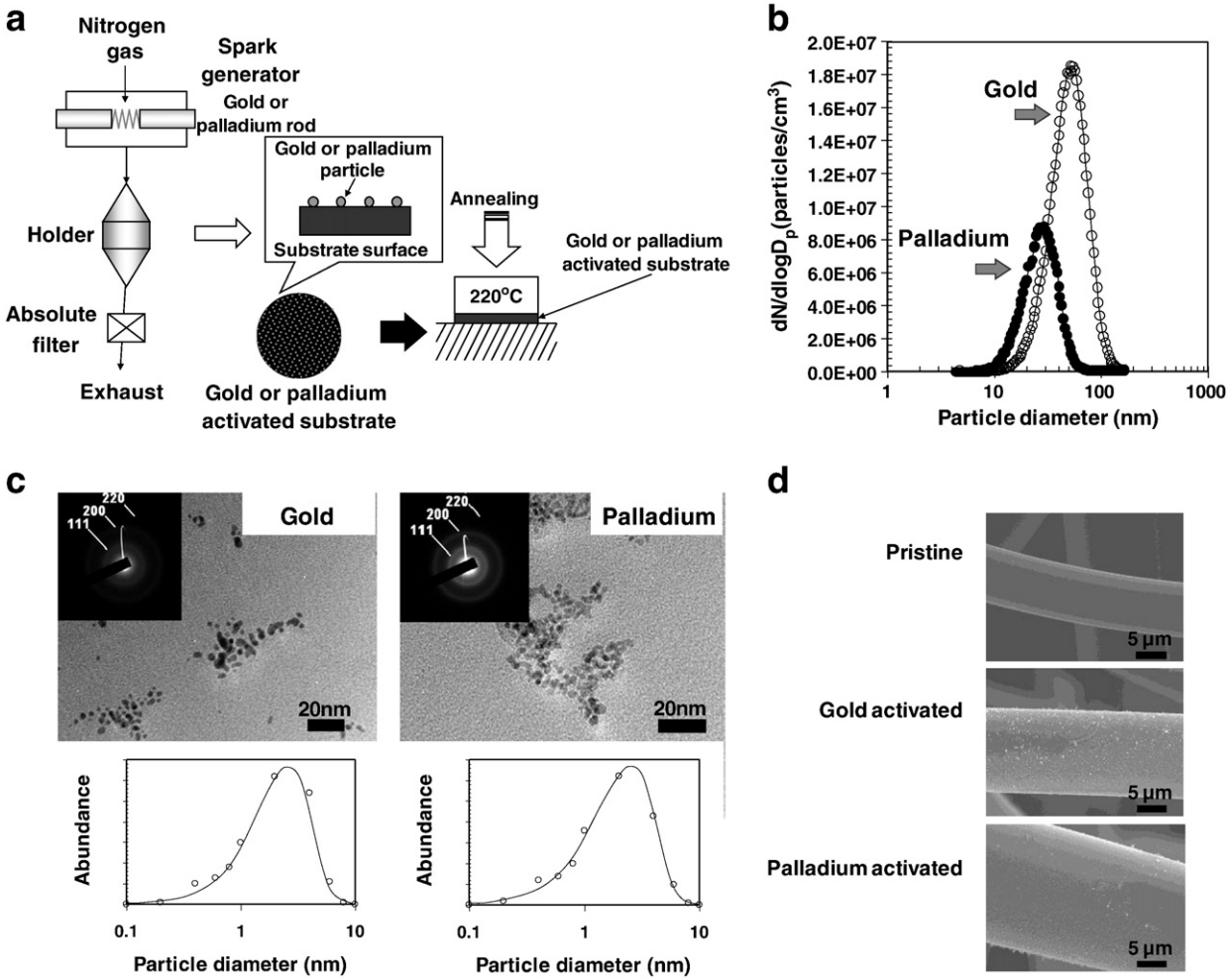

Fig. 1. Results of gold and palladium aerosol activations. (a) Diagram of aerosol activation. (b) Size distributions of spark produced particles. (c) TEM images and ED patterns. (d) SEM images of pristine and activated substrates.

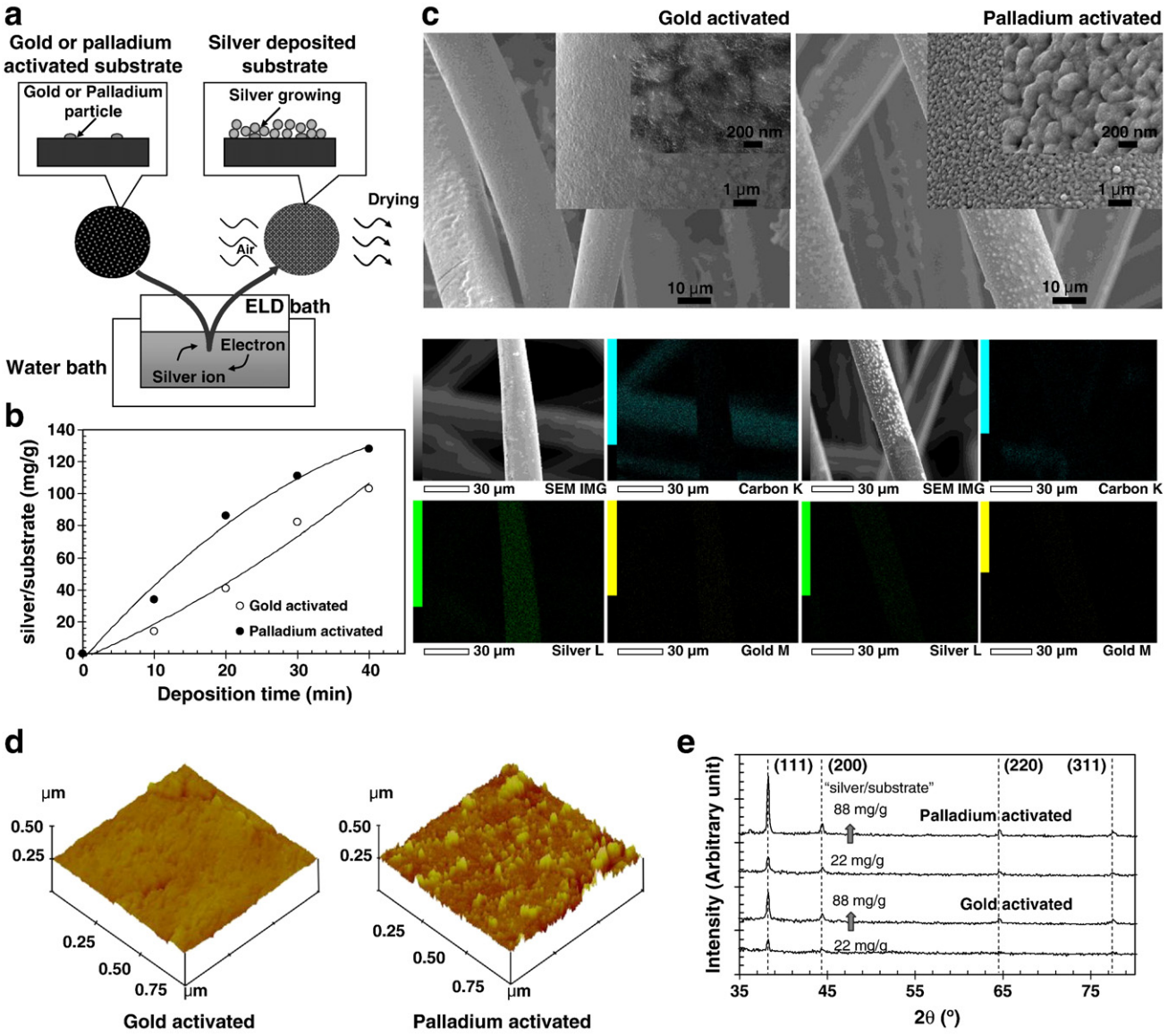

Fig. 2. Results of silver ELD. (a) Diagram of silver ELD. (b) Growth kinetics. (c) SEM images. (d) 3D AFM topographs. (e) XRD patterns.

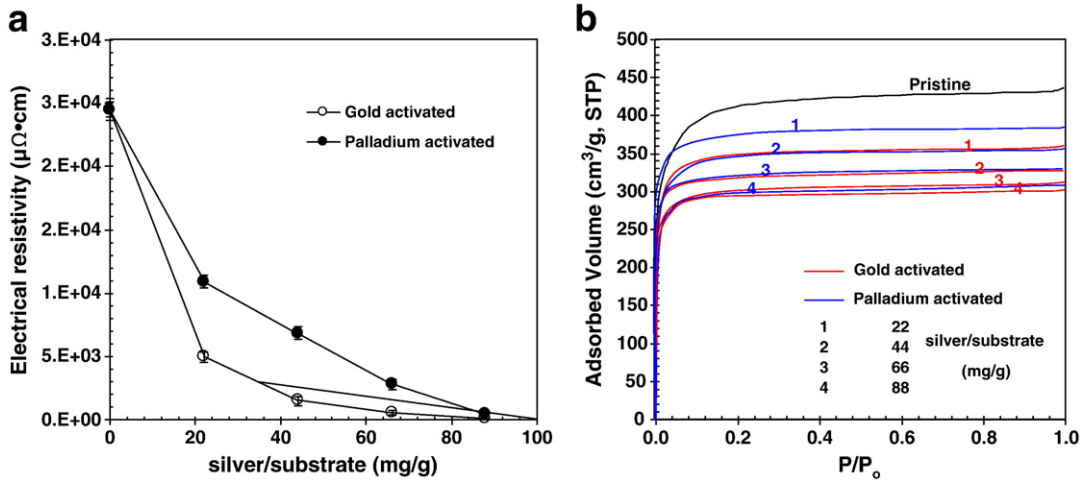

Fig. 3. (a) Electrical resistivities and (b) adsorption isotherms.

Table 2
Mass ratio of element in sample after ELD.

Silver/substrate (mg/g)	Element, wt%				
	Carbon	Oxygen	Gold	Palladium	Silver
	Activation, gold/palladium				
22	73.5/74.2	2.7/3.2	1.4/–	–/1.7	22.4/20.9
44	65.1/63.8	2.2/2.5	1.1/—	–/1.5	31.6/32.2
66	54.1/51.9	1.8/1.6	0.9/—	–/1.1	43.2/45.4
88	45.8/46.3	1.4/1.1	0.5/—	–/0.8	52.3/51.8

interval of 0.08°. An E scanner (NanoScope IIIa) having a maximum scanning size of 125 μm and a resolution of 0.02 nm was used. The drive frequency was 330 kHz, and the voltage was between 3.0 and 4.0 V. The drive amplitude was about 300 mV, and the scan rate was 0.5–1.0 Hz. Nitrogen adsorption isotherms of the PCF were measured using a porosimeter (ASAP 2010, Micromeritics Ins. Corp.) at −196 °C with a relative pressure ranging from 10^{-6} to 1.

3. Results and discussion

3.1. Size distribution and activation intensity

Figure 1b shows the size distribution of the spark produced gold (or palladium) aerosol nanoparticles, which was obtained using SMPS system. The geometric mean diameter (electrical equivalent mobility diameter) and geometric standard deviation were 48.8 (26.7) nm and 1.48 (1.43), respectively. The overall number and area concentrations were 7.75×10^6 (3.36×10^6) particles/cm^3 and 1.54×10^{10} (1.92×10^9) nm^2/cm^3, respectively. TEM image (Fig. 1c) shows that sizes of the spark produced nanoparticles were distributed around ~3.5 (2.6) nm (from inset of Fig. 1c) in primary particle diameter which was remarkably smaller than the size distribution in Fig. 1b and this means that the SMPS detected agglomerates of primary particles formed by self coagulation of primary particles [15,20]. The electron diffraction patterns (other inset of Fig. 1c) revealed characteristic rings in the polycrystalline diffraction pattern, which were all within 2% of the value reported for the (111), (200), (220), and (311) face-centered cubic (fcc) gold (or palladium) crystallites. From the above results, an activation intensity (I_a) [21] of substrate is defined as follows:

$$I_a = Q\cdot t_a\cdot m_s^{-1}\int_0^\infty \eta\left(D_p\right)C_a\left(D_p\right)dD_p \quad (1)$$

where, Q is the flowrate of nitrogen gas, t_a is the activation time, m_s is the mass of substrate, η (D_p) is the particle collection efficiency of PCF, and C_a (D_p) is the area concentration of gold (or palladium) nanoparticles. The gold (palladium) particle collection efficiency of PCF was 98.8% (98.2%), and indicated that a loss proportion of spark produced gold (palladium) particles was about 1% (2%) in number count. The activation intensity was selected approximately 3.8 x 10^2 mm^2/g (gold (or palladium)/substrate). Fig. 1d shows SEM images of the aerosol activated substrates. While pristine substrate had a clean surface, more particles were deposited on the substrates after both activations.

3.2. Silver coatings and characterization

Growth kinetics of silver was obtained from the ICPAES analyses (Fig. 2b), and the results revealed that the kinetics depends on activation material. Electrons transfer in silver ELD bath across palladium catalytic sites was better than that of gold, and thus decomposition of silver-amine complexes into silver metals were faster for palladium, resulting in faster growth kinetics. Fig. 2c shows low and high (insets) magnitude SEM images of silver deposited substrates for 88 mg/g (silver/substrate) in deposition amount from both activations. A uniform film with ultrafine particles (~12 nm in diameter) was observed without agglomeration and its microstructure can be clearly seen in the inset micrographs. While nodular particles (~132 nm in diameter) with agglomeration due to island growth were densely distributed for palladium activation but the coverage was not completed; some voids between the particles were seen on the substrate. A similarity of lattice parameter (refer to Table 1) between gold and silver induced layer-by-layer (LbL) growth, and thus surface uniformity and coverage for gold activation were better than those from palladium activation. Fig. 2c also shows the corresponding elemental results. The first image in each elemental result shows a different scaled image of the silver deposited substrate and following three images show the EDX maps for the first image. These maps corresponded to carbon, silver, and gold (or palladium), respectively. The dots in these images indicated the positions of each element in the first image. From the EDX qualifications (Table 2), it was found that the samples contained carbon, oxygen, gold (or palladium), and silver and their amounts were varied with deposition amount of silver. Atomic force microscopy 3D topographs of both activations are shown in Fig. 2d. It can be observed that the film was more distorted (root-mean-square (RMS) roughness of 44 nm) in palladium activation, while densely packed film has low roughness (RMS roughness of 8 nm) and lacks morphological features in gold activation. Generally, a LbL growth mode can be obtained at mild growth conditions while an island growth mode occurs at faster growth conditions. This might be another reason of the different roughness. Thereby, the experiments for observing the growth of silver at lower ELD bath temperature were performed to generate a mild growth condition even for activated by palladium, resulting in same growth kinetics with gold activation. Nevertheless, the film still had larger roughness (RMS roughness of 35 nm) than that for the gold activation, and it could be concluded that the lattice mismatch of palladium and silver might be the principal reason for the different roughness. XRD patterns (Fig. 2e) of the silver films reveal that the peaks corresponded to the (111), (200), (220), and (311) planes of the fcc phase of silver. Peak intensities of both activations increased with increasing the deposition amount. The peaks were comparatively broader when gold activation was applied because the broadening of peaks in the XRD patterns was generally related to smaller particle size.

Figure 3a shows electrical resistivity of silver deposited substrates from both activations. Resistivities (ρ) were calculated through the relationship as follows:

$$\rho = \frac{RA}{L} \quad (2)$$

where R, A, and L are the resistance, cross-sectional area, and length of the substrate, respectively. The substrate before silver ELD had an electrical resistivity of ~2.45×10^4 μΩ cm and the values after

Table 3
Textural properties of the PCF with silver films.

Silver/substrate (mg/g)	TSSA[a]	MSSA[b]	TPV[c]	MPV[d]	APD[e]
	Activation, gold/palladium				
Pristine	1624	1446	0.77	0.75	17.7
22	1259/1424	1142/1385	0.54/0.60	0.52/0.57	17.0/17.1
44	1111/1212	1044/1178	0.49/0.56	0.47/0.52	16.7/16.8
66	1094/1155	944/1014	0.46/0.52	0.45/0.49	16.3/16.2
88	942/1036	884/905	0.43/0.45	0.42/0.44	16.0/15.9

[a] Total specific surface area (m^2/g).
[b] Micropore specific surface area (m^2/g).
[c] Total pore volume (cm^3/g).
[d] Micropore volume (cm^3/g)
[e] Average pore diameter (Å)

silver ELD respectively ranged 4.9×10^3–64 and 1.1×10^4–498 μΩ cm for gold and palladium activations at 22–88 mg/g (silver/substrate) depositions (Table 2).With an increase of the content of silver, conductive paths among the particles increased, and the average distance between the particles became smaller; thus, the resistivity of the sample decreased. The values more rapidly decreased in gold activation with the increasing deposition amount due to a uniform film property. The resistivity of silver film was normally affected by some particle boundaries and defects [8], and thus the values from palladium activation were less sensitive. Fig. 3b shows that a major uptake of nitrogen occurred at a relatively low pressure ($P/P_0<1$) and a plateau was attained at $P/P_0\sim0.2$, implying that all the samples had microporous characteristics (type I isotherm), and details of the textural properties of the samples are summarized in Table 3. Even though a generation of surface area from the silver deposition (i.e. silver particle surface and void between silver particles) might occur simultaneously, the area was remarkably smaller (~20 m^2/g) than surface area of CFs (~1600 m^2/g) and pore size mainly ranged over microporosity, so the area generation from the deposition did not affect the decrease of microporosity. The early stage of the deposition, a larger porosity occupation was appeared with gold activation owing to the blocking and/or residence of pore inside and entrance with initially grown ultrafine silver particles on gold. On the other hand, a tendency of a smaller porosity decrease for gold activation carried over into the continuing deposition, which might be due to a lower porosity occupation with silver films from gold activation (i.e. planar deposition) than those from palladium activation (i.e. isotropic deposition). The LbL growth containing ultrafine silver particles from gold activation was also rather preferred for the porosity than island growth from palladium activation (Table 3).

Comparative characteristics were also briefly applied to copper ELD for both activations (Fig. 4), and following results (RMS roughness, nm: 33, gold vs 21, palladium and resistivity, μΩ cm: 524, gold vs 368, palladium) at 100 mg/g (copper/substrate) in deposition amount were also corresponded to degree of crystallographic misfit (refer Table 1) between activated surface and copper.

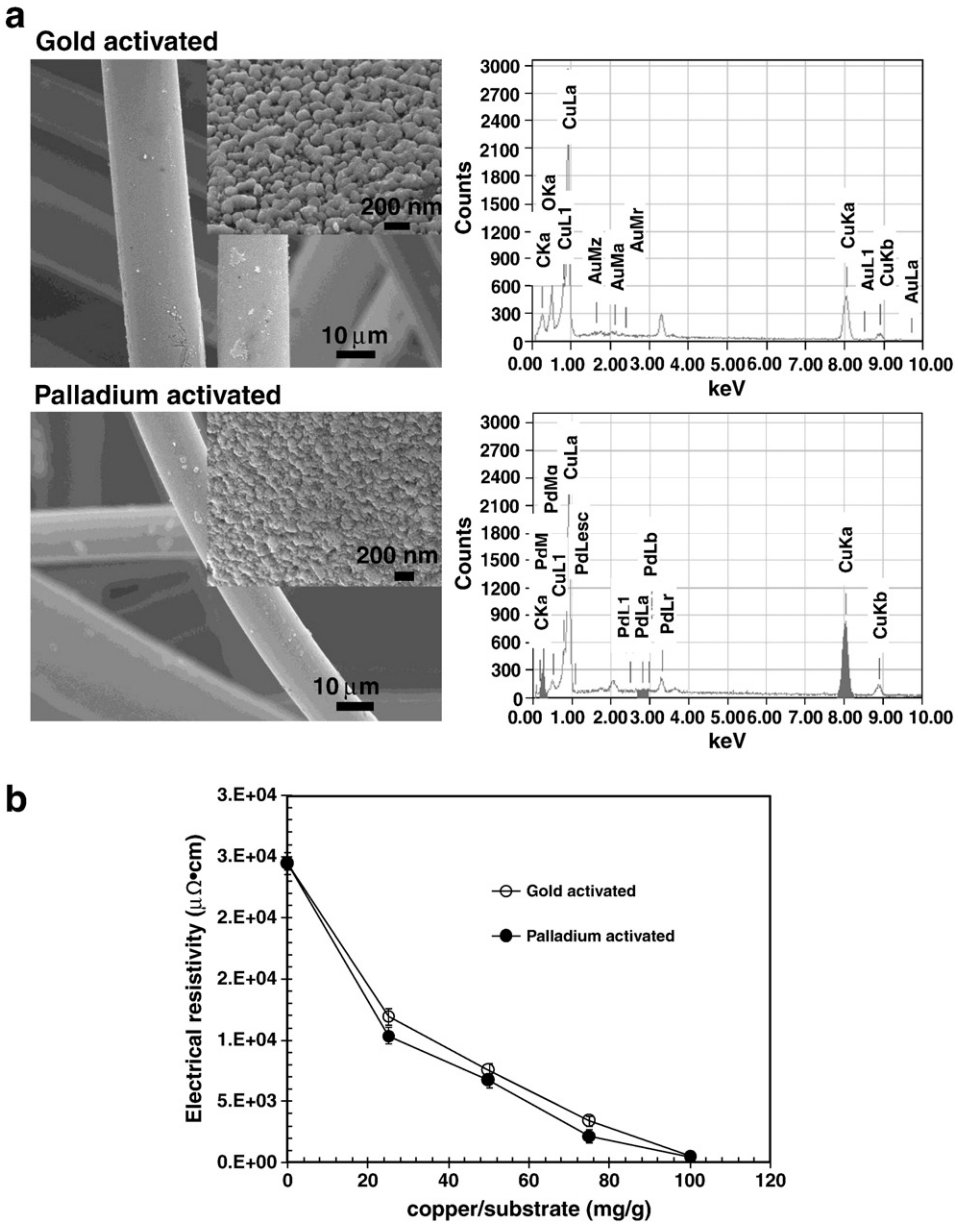

Fig. 4. (a) SEM images and EDX spectra of copper deposited substrates. (b) Electrical resistivities.

4. Conclusions

Using this gold aerosol activation and silver ELD processes, it was possible to create a flat silver film with a few nanometer roughnesses on a fiber substrate. Gold had a similar lattice parameter with silver in crystallinity and thus a crystallographic misfit between silver and gold activated surface was minimized during the ELD, resulting in a lower electrical resistivity than that from palladium activation. The investigated approach can be useful in fabrication of silver thin films on substrates and it is expected that such approach may have various applications in catalysis, plasmonic devices, sensors, and many other fields.

References

[1] S.S. Tzeng, F.Y. Chang, Thin Solid Films 388 (2001) 143.
[2] S.-S. Tzeng, F.-Y. Chang, Mater. Sci. Eng. A 302 (2001) 258.
[3] J. Suzuki, M. Yoshida, Y. Nishijima, K. Sekine, T. Takamura, Electrochim. Acta 47 (2002) 3881.
[4] J. Jang, S.K. Ryu, J. Mater. Process. Technol. 180 (2006) 66.
[5] X. Gan, Y. Wu, L. Liu, B. Shen, W. Hu, J. Alloys Compd. 455 (2008) 308.
[6] Y.-J. Oh, S.M. Cho, C.-H. Chung, Electrochem. Solid-State Lett. 8 (2005) C1.
[7] H. Bi, K.-C. Kou, K. Ostrikov, L.-K. Yan, Z.-C. Wang, J. Alloys Compd. 478 (2009) 796.
[8] S.H. Cha, H.-C. Koo, J.J. Kim, J. Electrochem. Soc. 152 (2005) C388.
[9] M.V. ten Kortenaar, J.J.M. de Goeij, Z.I. Kolar, G. Frens, P.J. Lusse, M.R. Zuiddam, E. van der Drift, J. Electrochem. Soc. 148 (2001) C28.
[10] J.J. Kim, S.H. Cha, Y.-S. Lee, Jpn. J. Appl. Phys. 42 (2003) L953.
[11] X. Zhao, K. Hirogaki, I. Tabata, S. Okubayashi, T. Hori, Surf. Coat. Technol. 201 (2006) 628.
[12] A. Inberg, L. Zhu, G. Hirschberg, A. Gladkikh, N. Croitoru, J. Electrochem. Soc. 148 (2001) C784.
[13] J.H. Byeon, J.-W. Kim, Langmuir 26 (2010) 11928.
[14] J.-P. Borra, J. Phys. D Appl. Phys. 39 (2006) R19.
[15] J.H. Byeon, J.H. Park, J. Hwang, J. Aerosol Sci. 39 (2008) 888.
[16] K. Ostrikov, A.B. Murphy, J. Phys. D Appl. Phys. 40 (2007) 2223.
[17] M. Keidar, I. Levchenko, T. Arbel, M. Alexander, A.M. Waas, K. Ostrikov, Appl. Phys. Lett. 92 (2008) 043129.
[18] J. Chen, G. Lu, L. Zhu, R.C. Flagan, J. Nanopart. Res. 9 (2007) 203.
[19] J.H. Byeon, J.H. Park, K.Y. Yoon, J. Hwang, Nanoscale 1 (2009) 339.
[20] J.P. Borra, Plasma Phys. Control. Fusion 50 (2008) 124036.
[21] J.H. Byeon, B.J. Ko, J. Hwang, J. Phys. Chem. C 112 (2008) 3627.